

A host-derived viral transporter protein for nitrogen uptake in infected marine phytoplankton

Adam Monier^{a,b,1}, Aurélie Chambouvet^{a,c,2}, David S. Milner^{a,2}, Victoria Attah^a, Ramón Terrado^d, Connie Lovejoy^{b,e}, Hervé Moreau^f, Alyson E. Santoro^g, Évelyne Derelle^f, and Thomas A. Richards^{a,1}

^aLiving Systems Institute, School of Biosciences, College of Life and Environmental Sciences, University of Exeter, Exeter, EX4 4QD, UK; ^bQuébec Océan, Université Laval, Québec, QC G1V 0A6, Canada; ^cLaboratoire des Sciences de l'Environnement Marin (LEMAR), UMR6539 UBO/CNRS/IRD/IFREMER, Institut Universitaire Européen de la Mer (IUEM), Technopole Brest Iroise, 29280 Plouzané, France; ^dDepartment of Biological Sciences, Dornsife College of Letters, Arts and Sciences, University of Southern California, Los Angeles, CA 90089-0371, USA; ^eTakuvik international laboratory (CNRS UMI 3376), Département de Biologie and Institut de Biologie Intégrative et des Systèmes, Université Laval, Québec, QC G1V 0A6, Canada; ^fCNRS UMR 7232, Sorbonne Universités, Observatoire Océanologique de Banyuls, 66650 Banyuls-sur-mer, France; ^gDepartment of Ecology, Evolution, and Marine Biology, University of California, Santa Barbara, CA 93106, USA

This manuscript was compiled on June 22, 2017

Phytoplankton community structure is shaped by both bottom-up factors such as nutrient availability, and top-down processes, such as predation. Here we show that marine viruses can blur these distinctions, being able to amend how host cells acquire nutrients from their environment while also preying and lysing their algal hosts. Viral genomes often encode genes derived from their host. These genes may allow the virus to manipulate host metabolism to improve viral fitness. Here we identify in the genome of a phytoplankton virus, which infects the small green alga *Ostreococcus tauri*, a host-derived functional ammonium transporter. This gene is transcribed during infection and when expressed in yeast mutants the viral protein is located to the plasma membrane and rescues growth when cultured with ammonium as the sole nitrogen source. We also show that viral infection alters the nature of nitrogen compound uptake of host cells, by both increasing substrate affinity and allowing the host to access diverse nitrogen sources. This is important because the availability of nitrogen often limits phytoplankton growth. Collectively, these data show that a virus can acquire genes encoding nutrient transporters from a host genome and that expression of the viral gene can alter the nutrient uptake behavior of host cells. These results have implications for understanding how viruses manipulate the physiology and ecology of phytoplankton, influence marine nutrient cycles and act as vectors for horizontal gene transfer.

Phycodnaviridae | NCLDV | Prasinophytes | Mamiellophyceae | Horizontal / Lateral Gene Transfer

Phytoplankton underpin the biogeochemistry of the surface oceans and drive the marine carbon and nitrogen cycles [1]. Nutrients fuel cyanobacteria and eukaryotic single-celled algae with the elements essential for organic matter biosynthesis, especially nitrogen (N) and phosphorus (P); hence nutrient availability exerts a bottom-up control on phytoplankton cell growth and oceanic productivity [2, 3]. In particular, N and P are found in low concentrations over much of the open ocean, limiting phytoplankton growth rates. Nutrient limitation, including co-limitation by several nutrients, results in competition among phytoplankton. In oligotrophic environments, and transiently nutrient depleted environments, phytoplankton species have evolved a range of strategies to optimize nutrient acquisition [4]. The genetic repertoire of N and P transporters show evidence of gene duplication, differential loss and horizontal gene transfer (HGT) in phytoplankton genomes as well as contrasting gene expression levels [5–9] suggesting that the evolution of these genes has been driven by adaptation to environmental limitation. Ammonium (NH₄⁺) and nitrate (NO₃⁻) are commonly available N source for marine phytoplankton

[10, 11] and, as such, the gene repertoire of cyanobacterial and eukaryotic phytoplankton are configured towards utilization of these two forms of inorganic N [12].

In addition to bottom-up nutrient limitation, phytoplankton community structure are influenced by top-down controls [13]. For phytoplankton communities these include predation by grazers and viral infection (see e.g., [14]). Marine viruses are the most abundant biological entities in the oceans; they are estimated to induce 10²⁸ infections daily [15] and are thought to control phytoplankton abundance, biomass and species composition through taxon-specific infections [16, 17]. There is a growing appreciation of the role of viruses in oceanic nutrient cycles, based on lytic infections leading to the release of dissolved and particulate organic matter, which is then recycled by other microorganisms [15, 18]. This virus-mediated process, referred to as the viral shunt, was suggested as a mechanism that maintains availability of organic matter in the euphotic zone by lysing cells before they sink [15, 18]. However, the influence of viruses on oceanic ecosystems extends beyond top-down host mortality. Genomic and metagenomic analyses show that marine viruses—either phages or eukaryotic viruses—harbor host-derived genes encoding a diverse range of putative functions [19–21], including whole biochemical pathways [22]. These ‘auxiliary metabolic genes’ (AMGs) may allow the virus to manipulate the host via metabolic reprogramming during infection, and have been experimentally shown to alter

Significance Statement

Viruses often carry genes acquired from their host. In the present work, we show that a virus of a marine alga carries a gene encoding a transporter protein that mediates nutrient uptake. We confirm that the viral transporter protein is expressed during infection and show that the protein functions to take up sources of nitrogen. This is important because acquisition of nutrients often determines the ecological success of phytoplankton populations. This work demonstrates how a virus can amend host-viral dynamics by modulating acquisition of nutrients from the environment.

A.M., D.S.M. and T.A.R. designed research; A.M., A.C., D.S.M., V.A. and E.D. performed research; A.M. analyzed data; H.M. and E.D. contributed reagents; A.M. and T.A.R. wrote the paper with contributions from all authors.

The authors declare no conflict of interest.

²A.C. and D.S.M. contributed equally to this work.

¹To whom correspondence should be addressed. E-mail: a.monier@exeter.ac.uk, or t.a.richards@exeter.ac.uk

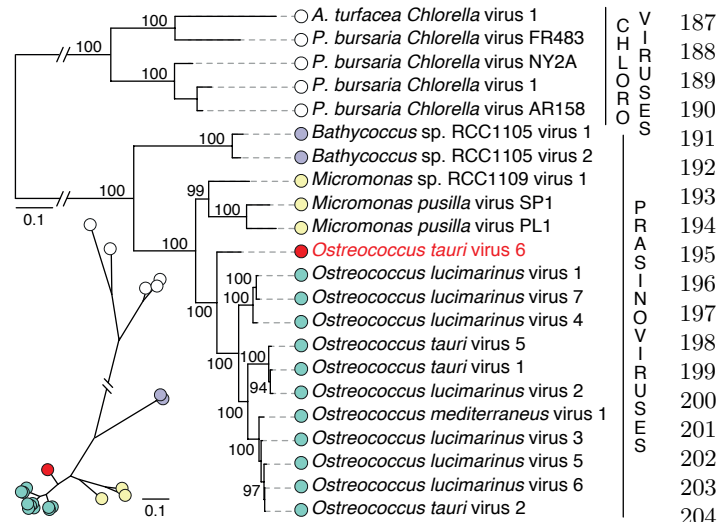
125 the central carbon metabolism and pigment biosynthesis of
 126 cyanobacteria [23, 24], and to ‘reprogram’ lipid biosynthesis of
 127 eukaryotic algal cells [25–27]. AMGs are thought to modulate
 128 host function to improve fitness of the virus and, in some
 129 cases, temporarily the host. For example, it was hypothesized
 130 that virally-encoded putative phosphate transporters increase
 131 accumulation of P in host cells [28, 29], which may in turn
 132 increase virus fitness given that P-depleted phytoplankton
 133 cells limit virus proliferation (e.g., [30, 31]).

134 Given the evidence of HGT for genes involved in both N
 135 and P metabolisms [7, 9, 32], the presence of host-derived
 136 phosphate transporters in phytoplankton viral genomes [29],
 137 and the importance of nutrient availability for phytoplankton
 138 and viral replication [33], we hypothesize that functional N
 139 transporters would also be found in genomes of phytoplankton
 140 viruses. Indeed, a recent analysis of marine viral metagenomes
 141 extended the catalog of functions encoded by AMGs, and
 142 reported the presence of genes putatively encoding NH_4^+ trans-
 143 porters in metagenomic assemblies which harbored phage genes
 144 [21]. To confirm the existence of potential virus-mediated N
 145 uptake processes, we searched available viral genomes for the
 146 presence of N transporters. Here, we report the identification
 147 of a host-derived N transporter harbored by an algal virus,
 148 OtV6. This virus infects the green alga *Ostreococcus tauri*
 149 and we show that the viral transporter is transcribed during
 150 the infection cycle. Cloning and phenotype analysis in yeast
 151 demonstrate that the viral protein transports NH_4^+ , methylam-
 152 monium and potentially a range of alternative N sources and
 153 that the viral transporter mediates a higher rate of methylam-
 154 monium uptake at low environmental concentrations compared to
 155 the *O. tauri* homolog. Algal culture experiments show viral
 156 infection alters host nutrient uptake dynamics during infection.

158 Results

159 **OtV6 genome harbors a putative NH_4^+ transporter.** To identify
 160 viral transporter proteins putatively involved in N uptake, all
 161 available viral amino acid sequences were screened using simi-
 162 larity searches based on hidden Markov models (HMM) encom-
 163 passing the main N transporter protein families. These HMM
 164 searches discovered a single viral protein potentially involved
 165 in direct N uptake. This viral protein sequence (UniProtKB
 166 [34] identifier: H8ZJB2) generated a significant hit with the
 167 Amt/Mep/Rh superfamily HMM (Fig. S1A). Members of this
 168 superfamily are integral membrane proteins involved in the
 169 electrogenic transport of ammonium ions, either the direct
 170 transport of NH_4^+ or ammonia (NH_3)/ H^+ co-transport [35].
 171 Several proteins from this superfamily have been shown to
 172 mediate the uptake of methylammonium, which can be used
 173 as a radiolabeled tracer ($^{14}\text{CH}_3\text{NH}_3^+$) to infer NH_4^+ uptake
 174 rates [36]. The viral transporter identified is encoded in the
 175 genome of OtV6, a virus belonging to the Phycodnaviridae
 176 family of nucleocytoplasmic large dsDNA viruses (NCLDV
 177 [37]). We name this viral putative NH_4^+ transporter vAmt
 178 (viral ammonium transporter).

179 Phycodnaviridae infect a broad range of eukaryotic algae
 180 [38]. To date, 12 genome sequences of viruses infecting the
 181 prasinophyte alga *Ostreococcus*—a widely distributed marine
 182 Mamiellophyceae [39, 40] and the smallest known free-living
 183 eukaryotic cell—are available [41–46]. These include viruses
 184 that infect one of three species: *O. tauri*, *O. lucimarinus*
 185 and *O. mediterraneus*. OtV6 infects a distinct population of
 186



205 **Fig. 1.** OtV6 branches basal to all other available *Ostreococcus* spp. viral genomes.
 206 ML phylogenetic tree of green algal viruses inferred from a concatenated sequence
 207 alignment of 22 core proteins shared among these viruses (7668 sites) under the
 208 LG+G+F model. The unrooted version of this tree is presented below the midpoint-
 209 rooted tree. A red circle indicates OtV6 branch; other colored circles represent
 210 the taxonomy of the viral hosts: green (*Ostreococcus*), purple (*Bathycoccus*), yellow
 211 (*Micromonas*) and white (chloroviruses, viruses of *Chlorella*, as outgroup clade).
 212 Node support was calculated from 1000 non-parametric bootstrap replicates; only
 213 bootstrap values > 90% are shown. The scale bar represents the number of estimated
 214 substitutions per site. The branch connecting the prasinoviruses to the chloroviruses
 215 was truncated for display.

216 *O. tauri* (shown to be resistant to another virus, OtV5 [44]),
 217 an alga originally isolated from a coastal NW Mediterranean
 218 lagoon [47].

221 **OtV6 is evolutionarily distinct from other *Ostreococcus*
 222 viruses.** To determine the phylogenetic position of OtV6
 223 among the Phycodnaviridae that infect green algae, we used
 224 the OtV6 genomic data [44] for a maximum-likelihood (ML)
 225 phylogenetic analysis. The ML tree reconstruction was based
 226 on a concatenated alignment of 22 conserved protein sequences
 227 [46] with a sampling of 7668 sites. In the resulting ML phy-
 228 logeny OtV6 branched at the base of all other *Ostreococcus*
 229 viruses (Fig. 1); both the basal position of OtV6 and the clus-
 230 tering of all other *Ostreococcus* viruses in a single clade were
 231 strongly supported (100% bootstrap support). This interme-
 232 diate phylogenetic position was also found in a ML phylogenetic
 233 tree of the viral DNA polymerase B (915 sites; Fig. S2) a
 234 gene commonly used as a marker for NCLDV phylogenetic
 235 and diversity analyses [48–50].

236 The phylogenies of both the viral core protein set and DNA
 237 polymerase B trees demonstrate that OtV6 is positioned al-
 238 most equidistant between the sampled *Ostreococcus* virus and
 239 *Micromonas* virus clades. By comparing the amino acid conser-
 240 vation levels of the 250 open reading frame (ORF) sequences
 241 of OtV6 with those of the other 11 *Ostreococcus* viruses and 3
 242 *Micromonas* viruses, we found that 20% of OtV6 ORFs were
 243 more similar to *Micromonas* virus homologs than to ones from
 244 *Ostreococcus* viruses (Fig. S3). In addition, 13 OtV6 ORFs
 245 had homologs in the genomes of *Micromonas* viruses, which
 246 were absent from all other *Ostreococcus* viruses. Given current
 247 sampling of Phycodnaviridae genomes, these results suggest
 248 that OtV6 represents an intermediate prasinovirus lineage.

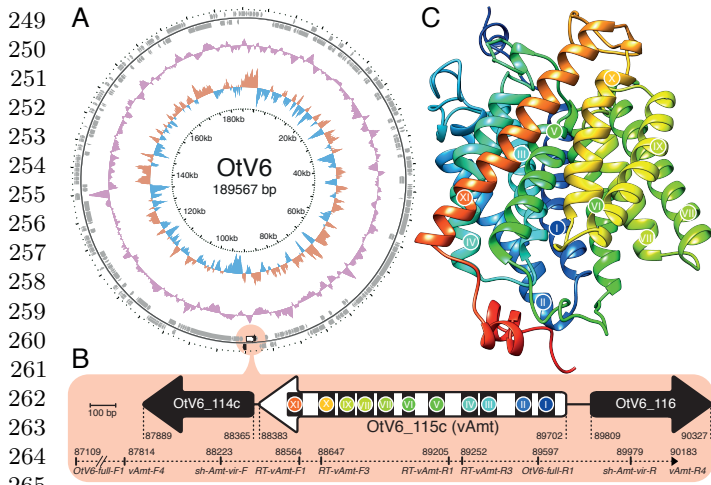


Fig. 2. vAmt genomic context and putative protein structure. (A) Circular depiction of the OtV6 genome. Oriented ORFs are mapped in grey on the outer ring. The light red circle indicates the vAmt locus along with neighboring ORFs. The colored plots drawn as intermediate rings display the biases in dinucleotide usages across the OtV6 genome: the red and blue plot shows the A+T skew, and the mauve plot shows the G+C content. (B) vAmt locus and neighboring ORFs. A white arrow represents the vAmt ORF (OtV6_115c), and black arrows represent the 5' and 3' vAmt flanking ORFs (OtV6_114c and OtV6_116, respectively; Fig. S4 displays the phylogenies of these flanking ORFs demonstrating viral provenance). The 11 predicted transmembrane domains along the vAmt ORF are indicated by black rectangles with colored circles, and numbered with Roman numerals. ORF lengths were scaled according to the 100 bp scale bar. Genomic coordinates indicate the 5' and 3' boundaries of each depicted ORF. The PCR amplified region is represented by a dashed line along with the corresponding amplicon genomic coordinates. (C) vAmt protein structure prediction. The predicted protein structure is composed of 11 helices corresponding to the transmembrane domains indicated by colored circles and Roman numerals, as in panel B (see Fig. S6 for sequence and structural comparisons of both host and viral copies and Fig. S7 for TMHMM posterior probabilities).

vAmt is virally-encoded and expressed during infection. Sequence searches and ML phylogenetic tree reconstructions confirmed the viral provenance of both vAmt flanking genes (OtV6_114c and OtV6_116; Fig. S4). To rule out contamination and genome assembly artifact, we confirmed the presence of the vAmt encoding gene (OtV6_115c) on the OtV6 genome by targeted PCR amplification (Fig. 2A,B). Three sets of PCR primers were designed to amplify through the complete vAmt encoding gene and its 5' and 3' flanking genes (Fig. 2B; Table S1; GenBank identifier: KX254356). These results confirm that the transporter encoding gene is linked to viral genes OtV6_114c and OtV6_116 and therefore residing on the viral genome. In addition, no spliceosomal introns were identified in the vAmt encoding gene, while all *Ostreococcus* spp. homologs have one intron with the exception of *Ostreococcus* sp. RCC809, which has no introns (Fig. S1B).

Next, we sought to confirm that the vAmt encoding gene is expressed during infection. We isolated RNA from infected and uninfected *O. tauri* cultures in parallel. Two different sets of reverse transcription (RT) PCR primers directed against the vAmt encoding transcript (*RT-vAmt* primer sets; Fig. 2B; Table S1) amplified products in the infected cultures; no amplicons were found in the uninfected cultures (Fig. S5). We sequenced both RT-PCR amplicons from the infected cultures and confirmed that they corresponded to the vAmt encoding gene and that this viral gene is expressed during infection.

vAmt is a NH_4^+ transporter. The vAmt ORF is located on the reverse strand of the OtV6 genome (Fig. 2A) and encodes a putative protein of 439 amino acids. Sequence similarity searches of UniProtKB demonstrate the Amt1.1 sequence from the OtV6 host *O. tauri* (UniProtKB identifier: A0A096PA30) has the highest similarity with 75.8% amino acid similarity and 62.3% nucleotide identity (Fig. S6A). In the curated SwissProt database [34], the best match to the viral protein was *Arabidopsis thaliana* Amt1.3 sequence (Q9SQH9; 65.9% amino acid similarity with vAmt), which was shown to mediate NH_4^+ uptake in N-replete and N-deplete conditions [51].

The vAmt predicted protein secondary structure has 11 transmembrane domains, a structural feature shared by other NH_4^+ transporter proteins including the *O. tauri* Amt1.1 (Fig. 2B, Fig. S6A and Fig. S7). These transmembrane domains corresponded to 11 alpha-helices, which have been shown for several NH_4^+ transporters to cross the membrane making up a conserved hydrophobic pore and to contribute to the overall channel stability of the transporter, as revealed by crystal structures [52–54]. In addition, the vAmt has a predicted extracellular N-terminal and cytosolic C-terminal topology, a topology also found for eukaryotic Amt proteins [35] (Fig. S7; see fig. S1C for comparison of Amt homolog C-termini). Furthermore, vAmt possess another hallmark of NH_4^+ transporters: two conserved histidine residues in the hydrophobic pore consistently found in helices V and X (Fig. S6A), and shown to be essential for transport activity [55]. In addition to the high level of sequence conservation between the vAmt and its *O. tauri* Amt1.1 homolog, protein structures inferred from viral (Fig. 2C) and host (Fig. S6B) homologs showed a high level of structural similarity (Fig. S6C).

To confirm the vAmt is a functional transporter, we cloned the vAmt encoding gene (pAG416 GPD vAmt) and transformed it into the yeast *S. cerevisiae* mutant 31019b [56], which has had the three known native yeast NH_4^+ Mep transporters deleted (*mep1Δmep2Δmep3Δ*). We compared growth of this mutant with parallel cultures of the same strain but containing only an empty vector (pAG416 GPD) and under culture conditions where 100 or 500 μM NH_4^+ were available as the sole N source. Complementation of the yeast mutant with vAmt increased growth rate and culture density consistent with vAmt encoding a functional NH_4^+ transporter (Fig. 3A and S8A). For comparison we showed that addition of pAG416 GPD vAmt did not facilitate growth of the YNVW1 *S. cerevisiae* mutant [57], which has had its urea transporter *dur3* gene deleted (*dur3Δ*), on medium containing 100 or 500 μM urea as sole N source (Fig. S8), indicating that vAmt does not transport urea in addition to NH_4^+ . GFP tagging of either the vAmt C- or N-termini identifies a plasma membrane localization, with some additional patchy localization, in yeast (Fig. 3B). Similar patterns of localization have been reported for plant Amt transporters, when expressed and tagged in yeast [58].

Comparison of radiolabeled methylammonium uptake rates in yeast mutants (strain 31019b) complemented with either the vAmt encoding or the *O. tauri* Amt1.1 genes demonstrated that the viral variant encodes a protein mediating the uptake of methylammonium with a higher rate at lower concentrations, for example 50 - 100 μM , compared to its *O. tauri* homologous protein which showed an improved uptake rate at higher methylammonium concentrations (e.g., 500 μM ;

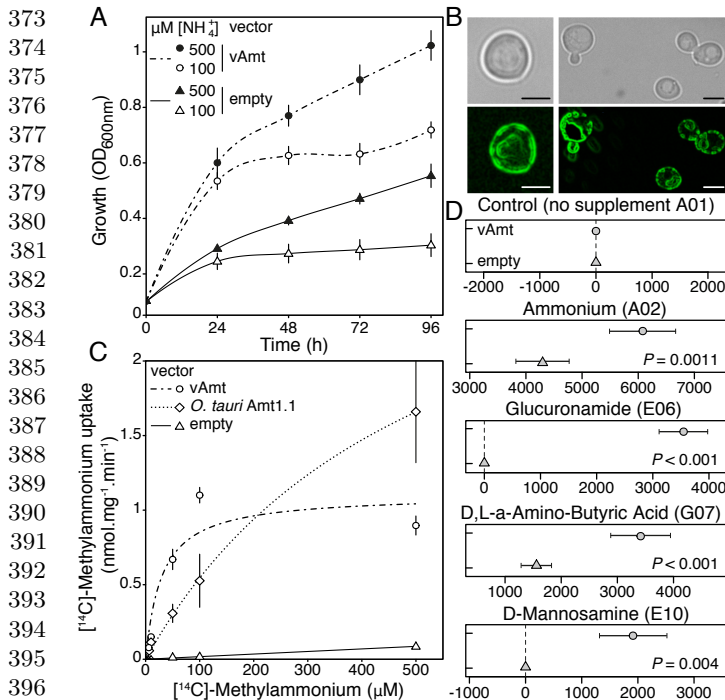


Fig. 3. vAmt is a functional NH₄⁺ transporter that takes up alternative substrates, is localized to the cell membrane and mediates an uptake at higher rate for low substrate concentrations than *Ostreococcus* Amt1.1 homolog when expressed in yeast. (A) Culture optical density (OD_{600nm}) of an NH₄⁺ uptake defective yeast mutant (strain 31019b) transformed either with an empty vector or a vAmt-containing vector in two NH₄⁺ concentrations (100 and 500 μM). Error bars represent standard errors based on culture triplicates. The lines represent local polynomial regression fits (see Fig. S8 for the equivalent results of an additional experiment with *O. tauri* Amt1.1). Growth of empty vector transformed mutant is facilitated by passive diffusion of NH₄⁺ across yeast membrane and/or scavenging of intracellular N stocks. (B) vAmt GFP fusion proteins expressed in yeast, cloned in-frame in N-terminus (left panel) or in C-terminus (right panel); scale bars display 3 μm distances. (C) [¹⁴C]-methylammonium uptake rates in mutant strain 31019b complemented with vAmt or the *O. tauri* Amt1.1 homolog. Lines show Michaelis-Menten curves; error bars represent standard errors based on culture triplicates. (D) OmniLog[®] comparison of mean point estimates and their 95% confidence intervals for N sources showing significant increase in respiration (area under the curve) of vAmt-transformed 31019b yeast cultures compared to non-vAmt transformed 31019b cultures; data was normalized by subtracting negative control. See Fig. S8 for complementation experiments confirming culture growth phenotypes in all of these results apart from D,L-a-amino butyric acid where complementation is not confirmed; see Fig. S9 for OmniLog[®] Phenotype Microarray respiration curves.

Fig. 3C). Strikingly, these analyses demonstrate that both transporter proteins have distinct substrate affinities and kinetics, specifically *O. tauri* Amt1.1 transporter has a K_m of 520 μM (± 250 s.e.; $V_{max} = 3.38 \pm 0.91$ nmol.mg⁻¹.min⁻¹) and the vAmt has a K_m of 30 μM (± 10 ; $V_{max} = 1.1 \pm 0.1$ nmol.mg⁻¹.min⁻¹). These distinct properties of host and viral transporters indicate that production of the vAmt protein during infection has the potential to alter the N uptake dynamics of infected cells.

Using the OmniLog[®] system [59], we investigated the range of N substrates that showed an increased respiration rate phenotype in yeast. Comparisons of the NH₄⁺-uptake deficient 31019b strain carrying pAG416 GPD vAmt with 31019b carrying only an empty vector (pAG416 GPD) were used to identify potential alternative substrates of the vAmt transporter that resulted in increased respiratory rates. In addition to NH₄⁺, this phenotype assay identified a significant increase in respira-

tory rate on three alternative N sources: D,L-a-amino-butyric acid, glucuronamide and D-mannosamine (Fig. 3D and Fig. S9). Two of these three alternative vAmt substrates were further confirmed by functional complementation experiments in yeast cultures (Fig. S8). We note that this method likely underestimates the range of substrates transported by vAmt because alternative substrates may have no 'metabolic' effect in yeast but could be utilized in other cellular background such as *O. tauri*.

Viral infection alters the uptake rate of methylammonium by *Ostreococcus* cells. Next we carried out infection experiments of *O. tauri* cultures with OtV6, in order to determine if infection and expression of the vAmt encoding gene altered the NH₄⁺ uptake rates of the host alga (relative to non-infected, control cultures; $n = 3$). To this aim, we conducted an infection timecourse experiment. For 16 hours post infection (hpi), we monitored *O. tauri* and virus-like particle (VLP) abundances (enumerated by flow cytometry; FCM) and methylammonium uptake rates (Fig. 4, Tables S2 and S3).

Based on FCM estimates of cell and VLP abundances, the ratio OtV6 particle to *O. tauri* cell (as a proxy for multiplicity of infection [60]) at the start of the experiment was of 0.42 ± 0.06 s.e.; algal growth was not significantly affected by viral infection for the first 12 hpi (Fig. 4A). At 12 hpi, temporal change in cell abundance significantly differed between control and infected algal cultures (two-sample t-test, $t_4 = 7.03$, $P = 0.002$; Table S2), with a sharp decrease of 11.8% on average in abundance for the infected cultures (corresponding to a loss of 0.59×10^7 .cells.ml⁻¹ ± 0.12 s.e.); in contrast, the control *O. tauri* cultures were steadily growing, with an average gain of 33% between 8 and 12 hpi (a gain of 1.44×10^7 .cells.ml⁻¹ ± 0.53). This drop in *O. tauri* cell number in infected cultures indicate occurrences of cell burst and lysis caused by viral shedding. The OtV6 latent period is thus between 8 and 12 hpi, a time frame comparable to other prasinovirus of *Ostreococcus* and *Micromonas* spp. [31, 41]. FCM enumeration of VLPs confirmed the reduction in VLPs prior to 12 hpi, consistent with virus adsorption followed by increase in VLPs after 12 hpi, which is in turn consistent with OtV6 particle release (Fig. 4A; Table S3).

During the infection experiment, we used two methods to track NH₄⁺ flux in *O. tauri* cells. First, we determined [¹⁴C]-methylammonium uptake rates of standardized subsamples of *O. tauri* cells throughout the timecourse experiments. This analysis demonstrated significant increases in methylammonium uptake rates for infected cells, consistent with viral infection altering the NH₄⁺ uptake phenotype of the phytoplankton host (Fig. 4C). We also monitored by fluorometry NH₄⁺ concentration in the cell-free culture media, which showed depletion at 8 hpi in NH₄⁺ concentration compared to 0 hpi in the infected cultures, although not significant (Fig. S10).

In addition, we used quantitative PCR (qPCR) to quantify the transcript levels of several *O. tauri* and OtV6 genes (Table S4) during the latent period of infected cultures (i.e., 0 - 12 hpi). The qPCR shows that transcription of the vAmt encoding gene is maintained relatively constant during infection, and at a similar level to that of the viral DNA polymerase B gene, while transcription of the gene encoding the major capsid protein increases until 4 hpi and is then expressed at relatively high level throughout 4 to 12 hpi (Fig. 5). Taken together, VLP and host cell dynamics, along with gene transcription, all

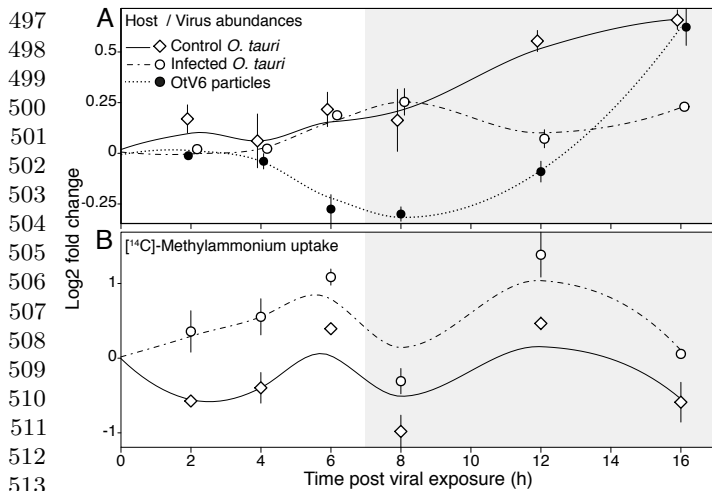


Fig. 4. Nitrogen source uptake during viral infection. (A) Temporal dynamics of host cell and viral particle abundances, and (B) [¹⁴C]-methylammonium uptake rates in OtV6-infected and non-infected *O. tauri* cultures. Three *O. tauri* cultures were exposed to OtV6 (timepoint 0 hpi) and three other non-infected cultures were used as controls. For each panel, (log₂) fold changes are based on timepoint 0 hpi (i.e., time of viral inoculation for infected *O. tauri* cultures); plots summarize the fold change distribution of three cultures for a given timepoint during the experiment, and trend lines were estimated by local polynomial regressions (loess). Shaded overlays indicate incubator dark period ('night'). *O. tauri* cells and virus-like particles were enumerated using flow cytometry; uptake rates were estimated by tracing the isotope labeled [¹⁴C]-methylammonium uptake in cultures taken as subsamples throughout the timecourse experiment. See Tables S2 and S3 for two-sample t-test results.

indicate a substantial viral infections of *O. tauri* cells resulting in an altered methylammonium uptake phenotype.

OtV6 acquired vAmt from an *Ostreococcus* host. We sought to explore the ancestry of the vAmt encoding gene by conducting phylogenetic tree reconstruction using a comprehensive sampling of protein sequences of the Amt/Mep/Rh superfamily (Fig. 6A). Proteins of this superfamily are found across all three domains of life and are involved in the transport (uptake and excretion) of ammonium ions through cell membranes [35]. This superfamily of membrane proteins has a complex evolutionary history marked by gene duplications, losses and HGT events, probably driven by environmental selection linked to N availability [7, 32]. In a phylogenetic study, McDonald and colleagues updated the Amt/Mep/Rh superfamily phylogeny [32], showing a partitioning into distinct clades: the monophyletic groups 'Amt-Euk' (originally named Amt1) and 'Mep', as well as two distantly related clades, 'Rh' (Rhesus) and a cluster of archaeal and bacterial homologs grouped into 'Mep-grade'. The Amt-Euk clade is composed of eukaryotic sequences, with a large representation of phytoplankton and plant species. For the host of OtV6, *O. tauri*, four Amt/Mep/Rh transporters were identified in its genome [7], two Amt-Euk (eukaryotic origin; Amt1.1 and 1.2) and two Mep_α (probably acquired via HGT; Amt2.1 and 2.2).

To determine which clade the vAmt groups within, a large-scale, approximate ML phylogenetic tree reconstruction was conducted based on an alignment of all available, non-redundant Amt/Mep/Rh protein sequences, including those from the marine microbial eukaryotic transcriptome project (MMETSP [61]; which includes several *Ostreococcus* transcriptomes such as *O. mediterraneus*). The resulting Amt/Mep/Rh superfamily phylogeny (based on an alignment of 374 sites;

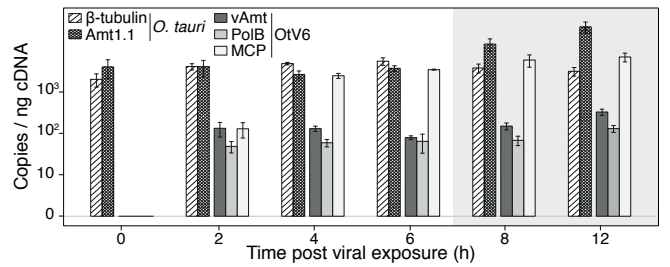


Fig. 5. OtV6-infected *O. tauri* gene expression. Transcript levels were RT-qPCR monitored in infected *O. tauri* cultures ($n = 3$; same infected cultures as presented in Fig. 4), and expressed as copies per ng of cDNA library (displayed on a log₁₀ scale, Y-axis). Hatched bars show transcript copy numbers of two *O. tauri* genes (β -tubulin and the NH₄⁺ transporter Amt1.1); solid color bars show copy numbers for three OtV6 genes (dark grey: viral NH₄⁺ transporter, vAmt; light grey: DNA polymerase B; white: major capsid protein). Error bars represent standard errors. Shaded overlays indicate incubator dark period ('night').

Fig. 6A and Fig. S10) demonstrates that the vAmt branched within the Amt-Euk clade. To determine the branching position of the vAmt sequence more accurately, a ML phylogenetic tree was reconstructed using a subset of Amt-Euk homologs (364 sequences, alignment comprised of 429 sites; Fig. 6B and Fig. S11). This phylogeny shows the vAmt branching with the *Ostreococcus* Amt1.1 family radiation, demonstrating that the OtV6 vAmt encoding gene is derived from its host lineage, most likely via host-to-virus HGT. In addition to the recent identification of putative Amt transporters on phage contigs assembled from marine metagenomes [21], our phylogenetic analyses also demonstrated that two metagenomic sequences retrieved from the viral fraction of aquatic samples (Pacific solar salterns, San Diego, USA [62]) branch with the OtV6 vAmt (Fig. 6B and Fig. S11), suggesting a wider geographical distribution of viral NH₄⁺ transporters.

Discussion

Here, we demonstrate that a virus of the marine phytoplankton *O. tauri*, representing a distinct lineage of *Ostreococcus* virus (Fig. 1), harbors a gene encoding a transporter protein that is expressed during infection (Fig. 5 and S5) and functions to take up NH₄⁺ (Fig. 3A and S8A) and a range of alternative fixed N sources (Fig. 3D, S8 and S9). Phylogenetic analyses show that the viral transporter is the result of a HGT event and was acquired from the host *Ostreococcus* lineage (Fig. 6B).

Viral HGT and functional compatibility. Many host-derived AMGs, including the vAmt encoding gene reported here, are highly similar at the sequence level to their host homologs. This has two implications: first, it complicates the analysis of viral metagenomes, as the process of host-to-virus HGT is likely to 'contaminate' viral metagenomes with sequences that appear as though they should belong to larger sample filtration fractions (i.e., the fraction containing host genomes). This can be ameliorated by the use of metagenome assembly methods that control for host-derived genes harbored by viral genomes [21]. Second, it confirms that viruses are acquiring genes from their host lineage and therefore acting as vectors for HGT. HGT and viral integration of genes that function in how host cells interact with their environment demonstrates a selective scenario that can drive transfer of genes encoding functional traits. Indeed, bacterial genomic islands often

621 contain transporter encoding genes and have been shown to
 622 undergo gene gain at high relative rates (for instance in the
 623 pico-cyanobacterium *Prochlorococcus* [63]). Genes that en-
 624 code transporter proteins are relevant because they encode the
 625 proteins responsible for nutrient uptake and are *functionally*
 626 *compatible*. We define a *functionally compatible* gene as a
 627 single gene that encodes a complete trait and also requires
 628 little protein-protein interaction network complexity to result
 629 in a function [64, 65]. As such, these gene classes are easily
 630 lost, duplicated or (re-)acquired during the diversification of a
 631 lineage, leading to these genes having complex evolutionary
 632 histories often involving HGT events [7, 29, 32, 66], as simi-
 633 larly observed for photosynthesis genes harbored by genomes
 634 of marine cyanophages [67–69].

635
 636 **The role of vAmt during infection.** Both *O. tauri* and *O. luci-*
 637 *marinus* are able to grow with NH_4^+ as the sole N source [70].
 638 Here we demonstrate that the vAmt encoding gene harbored
 639 by OtV6 is transcribed during viral infection (Fig. 5 and
 640 Fig. S5), and NH_4^+ (methylammonium) uptake in infected
 641 *Ostreococcus* cells is enhanced compared to uninfected cells
 642 (Fig. 4C). Interestingly, expression in a yeast mutant demon-
 643 strates that the viral vAmt transporter has a higher affinity
 644 (defined here as [^{14}C]-methylammonium uptake rate) at low
 645 environmental substrate concentrations compared to the algal
 646 transporter homolog, which has a higher relative NH_4^+ uptake
 647 rate at higher environmental concentrations. Competition for
 648 NH_4^+ is fierce in many marine systems, given that it is often
 649 the preferred source of inorganic N for phytoplankton cells
 650 [10]. Expression of the vAmt encoding gene during *O. tauri*
 651 infection may increase host NH_4^+ uptake rate and therefore may
 652 provide an advantage to infected host cells over non-infected
 653 algae in terms of N uptake, allowing an infected population
 654 to temporarily out-compete other phytoplankton species in-
 655 cluding uninfected sister cells. As such, production of vAmt
 656 transporter proteins is likely to act to fulfill the extended N
 657 requirements of viral replication within the infected host cell
 658 to sustain the physiological burden of viral replication through
 659 the uptake of various organic N sources.

660 Using comparative culture screening, we show that the
 661 vAmt protein potentially mediates the uptake of alternative
 662 organic N sources in addition to NH_4^+ . Amt transporter pro-
 663 teins are known to mediate the uptake of at least one al-
 664 ternative to NH_4^+ , methylammonium [71]. Most knowledge
 665 regarding substrate affinities of protein transporters derives
 666 from annotation resulting from sequence homology searches,
 667 and few experimental studies; it is thus important to take
 668 into account, when assessing the significance of transporter
 669 proteins in an ecological context, that these proteins may
 670 display affinities to additional substrates not described via
 671 bioinformatic annotation [72].

672
 673 **Viral manipulation of host elemental composition.** Harboring
 674 genes coding for functional nutrient transporters implies that
 675 phytoplankton viruses directly manipulate the elemental com-
 676 position of their host cells. This viral stoichiometric alteration
 677 would confer a strong advantage to viruses able to interfere
 678 with the hosts' nutrient uptake capabilities by encoding their
 679 own transporter repertoires. Availability of nutrients to phy-
 680 toplankton hosts has been shown to be of critical importance
 681 for phytoplankton virus proliferation (see [33]). Infection ex-
 682 periments on phytoplankton cultures depleted in P and N

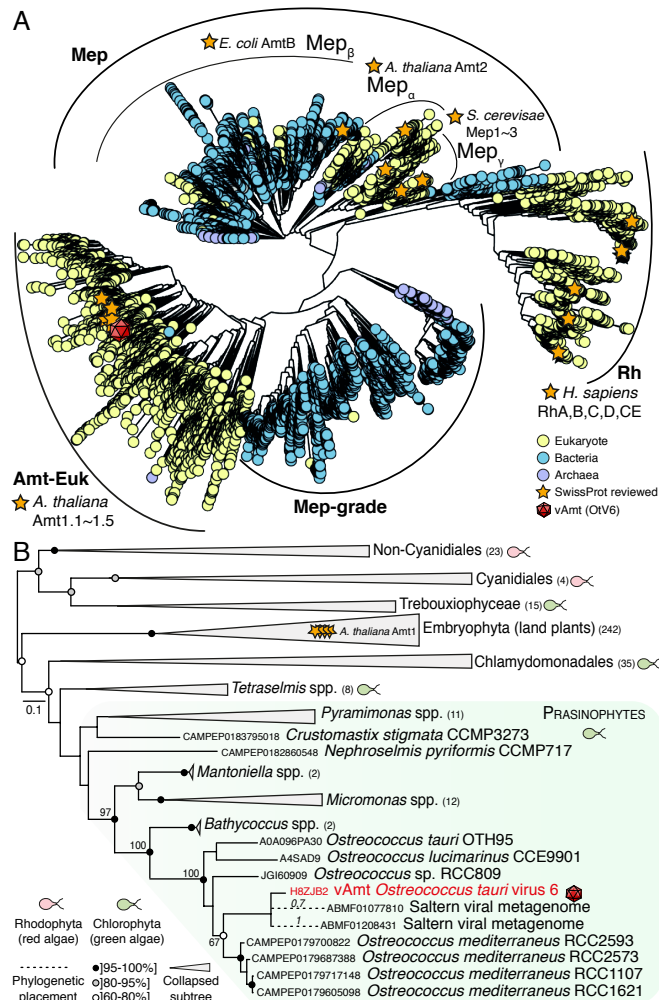


Fig. 6. vAmt phylogenetic ancestry shows it is derived by HGT from the host lineage. (A) Amt/Mep/Rh superfamily phylogenetic tree. This large-scale approximate ML tree was inferred under WAG+G model. Homologs were recruited based on a similarity search using the Pfam HMM corresponding to the Amt/Mep/Rh superfamily (PF00909) against UniRef100 (i.e., non-redundant version of UniProtKB), MMETSP protist transcriptomes and predicted proteomes from various protist genome projects; the final curated alignment was composed of ~20k protein sequences encompassing 374 sites. Curved black lines indicate the phylogenetic positions of the main clades (Amt-Euk, Mep, Mep-grade and Rh) as well as Mep subclasses (α , β and γ). The red capsid graphics shows the phylogenetic position of the vAmt within the superfamily tree, positioned within the Amt-Euk clade. For contextual reference, orange stars represent SwissProt reviewed protein entries; yellow, blue and purple circles represent eukaryotic, bacterial and archaeal proteins, respectively. See Fig. S10 for additional information, including local support values, MMETSP sequence positions and scale bar. (B) vAmt evolutionary relationships with Amt-Euk (Amt1) homologs. This ML phylogenetic tree was inferred under LG+I+G+F model, based on a multiple alignment of 364 proteins totaling 429 sites. These vAmt homologs were recruited and selected based on the Amt/Rh/Mep superfamily phylogenetic tree reconstruction. Green and red cell schematics represent green and red algal lineages. vAmt is highlighted in red with a capsid graphics, and branched within the prasinophyte green algae, delimited by a green frame. Code numbers in front of species names represent sequence identifiers from either the MMETSP transcriptomes (*O. mediterraneus*, *N. pyriformis* and *C. stigmata*), UniProtKB (*O. lucimarinus* and *O. tauri*) and the *Ostreococcus* sp. RCC809 genome project available at the DoE-Joint Genome Institute. Numbers in parentheses besides clade names are the number of sequences present in collapsed nodes. Branch node supports were computed from 1000 non-parametric bootstrap replicates. Grey and black circles correspond to bootstrap values of [80 – 95%] and [95% – 100%], respectively. The dashed branches represent the phylogenetic placement of two short environmental sequences, with placement posterior probabilities indicated on their corresponding branches; both sequences originate from a saltern viral metagenome (NCBI BioProject: PRJNA28353), and their GenBank sequence identifiers are provided. See Fig. S11 for additional data and uncollapsed branch information.

745 have shown that low concentrations of these nutrients can
746 significantly hamper viral cycle dynamics in terms of latent
747 period and burst size (i.e., the number of viral progeny per
748 lysed cell) as well as decreasing the infectivity of viral proge-
749 nies; such constraints on viral replication has been shown for
750 various clades of Phycodnaviridae (e.g., [30, 73]), including for
751 a *Micromonas* virus, a close relative of OtV6 (Fig. 1).

752 Although most studies have focused on the effect of low P
753 availability on phytoplankton virus replication, recent studies
754 have shown the importance of N availability for the quality
755 of viral replication [31, 73]. In particular, the burst size of
756 PBCV1, a virus of the green alga *Chlorella*, was shown to
757 decrease with higher C:N ratio of the algal host cell [73]. Fur-
758 thermore, the effect of N depletion was shown to be more
759 detrimental to viral proliferation than low P availability for a
760 Phycodnaviridae-phytoplankton system [31]. These results are
761 somewhat anticipated because of the stoichiometric require-
762 ments of phytoplankton virus replication, which is exacerbated
763 by the strong discrepancy in C:N:P ratios between viral par-
764 ticle and the host phytoplankton cell [74]. Viruses exhibit
765 much lower C:P and C:N ratios than their hosts, as shown
766 for PBCV1's 17C:5N:1P composition [75], compared to the
767 Redfield ratio of 106C:16N:1P, the elemental composition of
768 an average phytoplankton [74].

769 In the case of the Phycodnaviridae EhV, a virus of the
770 coccolithophore *Emiliania*, it was noted that viral genomes
771 were being overproduced during the infection cycle, relative to
772 the number of capsids being produced by the infected phyto-
773 plankton [76]. Such discrepancy between genome and capsid
774 productions may be linked to a shortage in amino acids and/or
775 lipids, constituent of EhV lipid membrane, limiting viral pro-
776 duction [76, 77]. This is predictable for Phycodnaviridae given
777 the N requirements of PBCV1 capsid, which is composed of
778 ~5050 major capsid proteins (MCP; [78]). Based on the MCP
779 protein sequence of PBCV1, the elemental composition of
780 the complete PBCV1 capsid would be $C_{2161}H_{3301}N_{577}O_{657}S_9$,
781 that is, a C:N ratio of 4:1. Hence, the ability of OtV6 to
782 express its gene encoding vAmt and enhance or maintain NH_4^+
783 uptake would allow the host to fulfill the requirements in N
784 imposed by the viral replication, in turn providing a strong
785 fitness advantage to OtV6 relative to marine viruses without
786 a N transporter gene repertoire. Further work will be required
787 to understand the role of virally-encoded nutrient transporters
788 in the dynamics of viral replication, especially in contrasting
789 nutrient concentrations.

790
791 **Blurring top-down and bottom-up controls.** Consistent with
792 the idea that viral proteins act to amend host N metabolic
793 function, a putative glutamine synthetase gene has also been
794 identified in the genomes of NCLDVs such as Mimivirus and
795 Mamavirus [79]. These data suggest that viral reprogramming
796 of host N metabolism may be a wider phenomenon [21, 80],
797 as has been shown for photosynthetic function [81], sulfur
798 oxidation [82], lipid [25–27] and phosphate metabolism [83].
799 Evidence that a viral lineage can acquire host genes to amend
800 host nutrient uptake has implications for our understanding
801 of phytoplankton ecology. Specifically, this phenomenon blurs
802 the lines between bottom-up and top-down regulation of phy-
803 toplankton communities, because here a top-down viral agent
804 has acquired the host genes which allow it to amend phyto-
805 plankton nutrient acquisition from the environment, which is
806 normally considered a bottom-up process.

Materials and Methods

vAmt identification, sequence and structure analyses. To identify a
viral transporter sequence putatively involved in NH_4^+ uptake, all
protein sequences available in UniProtKB [34] and the NCBI non-
redundant Reference Sequence database [84] were searched using
'hmmsearch', part of the HMMer v3 software suite [85], with the
Pfam [86] HMM corresponding to the NH_4^+ transporter superfamily
(Pfam release 3.0 identifier: PF00909). Hits were filtered using
E-value ($1e^{-10}$) and gathering cutoffs. This large-scale search
identified only a single viral encoded putative transporter protein,
OtV6 vAmt (HMMer search statistics with PF00909 model: score:
418.4, E-value: $1e^{-129}$). To avoid missing additional putative viral
 NH_4^+ transporters –potentially due to inaccurate viral gene modeling–
a HMM based search was repeated on 6-frame translations of all viral
genomes available at the NCBI genomic sequence repository (ORF
minimal size: 60 amino acid residues). In addition to the Pfam-
based HMM searches, further searches using the TIGRfam [87] NH_4^+
transporter HMM (TIGR00836; release 15) were conducted using
the aforementioned protein sequence datasets. These additional
searches did not recover any other viral sequences matching the
 NH_4^+ transporter HMMs.

Transmembrane domains of the vAmt and *O. tauri* Amt1.1
protein sequences were identified using TMHMM v2 [88]. Protein
structures were predicted using I-TASSER v4.2 [89]; the C-scores of
the vAmt and *O. tauri* Amt1.1 3D structure models were 1.36 and
0.72, respectively. *O. tauri* Amt1.1 and vAmt predicted structures
were aligned using MatchMaker (UCSF Chimera [90]).

Phylogenetic tree reconstructions. The Amt/Mep/Rh superfamily
phylogeny was reconstructed using an approximate ML method as
implemented in FastTree v2.1 ([91]; compiled using the double pre-
cision flag) and based on an alignment of 19,493 protein sequences
sampled from UniProt100 (clustered at 100% sequence identity; [34]
in order to reduce redundancy). HMM searches were also conducted
against predicted protein sequences from the MMESTP transcrip-
tomic data [61] and from protist genome projects available at the
DoE-Joint Genome Institute. All identified putative Amt/Mep/Rh
sequences were then aligned using 'hmmalign' [85] and sequences
shorter than 50 amino acid residues were discarded. Alignment sites
composed of more than 50% of gaps were discarded. Mis-aligned
and/or false positive sequences were detected using preliminary
phylogenetic reconstructions with FastTree (default parameters).
Sequences that resulted in very long branches were then removed
allowing a final tree calculation using the 'accurate' mode (-slow) with
the WAG+G substitution matrix.

For the ML phylogeny, different strategies were applied for puta-
tive homolog sampling. For the viral DNA polymerase B and the
vAmt flanking ORFs, homologous protein sequences were identified
with BLASTP [92] similarity searches against UniProtKB. The
homologous sequences were then aligned using the iterative refine-
ment method E-INS-i as implemented in MAFFT v7.2 [93], edited
with trimAl v1.4 'strict' algorithm [94] and manually inspected
and corrected. For the phylogeny based on the 22 core proteins
shared among green algal viruses [46], the OtV6 predicted proteome
was parsed using BLASTP and homologous sequences from other
Ostreococcus spp. viruses were used as search queries. The resulting
22 OtV6 core proteins were then concatenated, aligned and added
to the original viral core protein alignment using MAFFT.

For the vAmt/Amt-Euk ML phylogenetic subtree, vAmt ho-
mologs were identified using the previous large-scale, superfamily
phylogenetic reconstruction described above. Sequences branching
with vAmt were identified; corresponding full-length sequences were
retrieved and aligned with MAFFT E-INS-i, and manually inspected.
After homolog sequence selection and alignment, the same method-
ology was applied for all ML phylogenetic tree reconstructions. The
most likely tree was identified from 100 ML reconstructions, using
RAxML v8.2 [95], and under the substitution model best fitting the
data, as identified by ProtTest v3 [96] using the Akaike information
criterion; branch support values were based on 1000 non-parametric
bootstrap replicates.

869 **Metagenome screening and phylogenetic mapping.** To investigate
870 the wider distribution of vAmt-like homologs, we screened
871 metagenomes for similar sequences in GOS, *Tara Oceans* giant
872 virus dataset [50] as well as all aquatic metagenomes available at
873 iMicrobe [97]. Putative vAmt homologs were aligned to alignment
874 MAFFT (without altering the original alignment) and then phyloge-
875 genetically mapped onto the ML tree using pplacer v1.1 [98]. Within
876 this tree, two Amt-Euk sequences mapped to the vAmt branch.

877 **vAmt genomic amplification.** To confirm the vAmt encoding gene
878 was harbored by OtV6, we designed specific primer pairs (listed
879 in Table S1) and the vAmt gene along with its 5' and 3' flanking
880 regions were amplified, represented by a ~2500 bp sequence. For
881 each PCR reaction, a negative control (distilled H₂O) was included.
882 PCR reactions (25 µL total volume) were conducted using GoTaq®
883 Green Master Mix (Promega, Madison, WI, USA) with 1 µL of virus
884 OtV6. Cycling reactions were as follows: 5 m at 95 °C, followed by
885 30 cycles of 30 s at 95 °C, 30 s at 54 °C, 120 s at 72 °C and with an
886 additional 10 m extension at 72 °C. The PCR reactions were checked
887 on 1% agarose gel stained with GelRed™ (Biotium, Hayward, CA,
888 USA). The positive PCR reactions were then directly cloned using
889 the StrataClone™ PCR cloning kit (Agilent Technologies, Santa
890 Clara, CA, US) according to the manufacturer's instructions. One
891 clone per library was selected and double strand sequenced using
892 universal *M13* primers. All amplicon sequencing was performed
893 externally by Eurofins Genomics (Ebersberg, Germany).

894 **Ostreococcus culture infection and vAmt RT-PCR.** *O. tauri* cells from
895 the RPN2 population (OtV5 resistant; see [44]) were grown in L1
896 medium exponentially under 12:12 light (32.3 photons µmol m⁻²
897 s; 1700 lux). Infection experiments proceeded as followed: 5 mL
898 of *O. tauri* at exponential growth were infected using 250 µL of
899 purified OtV6; as a negative control, 5 mL of *O. tauri* culture
900 were incubated with 250 µL of L1 medium. To test for the expression
901 of the vAmt encoding gene during the infection cycle, the *O. tauri*
902 cultures were sampled 12 h after OtV6 inoculation; 1 mL of the
903 infected and uninfected cultures were sampled and centrifuged at
904 8000 rpm during 10 m. After removal of the supernatant, the pellets
905 were flash frozen and stored at -80 °C. RNA was extracted using
906 the RNeasy® Plus Universal Kits (Qiagen, Valencia, CA, USA).
907 An extra step to remove all genomic DNA was added after the
908 RNA extraction protocol using the RTS DNase™ kit (MO BIO
909 Laboratories, Qiagen).

910 Using three sets of primers that amplify an overlapping region
911 of the vAmt encoding gene (*OtV6-full-F1/R1*, *vAmtF4/R4* and
912 *sh-Amt-vir-F/R*; Fig. 2B and Table S1), we first checked for the
913 presence of DNA contamination in the RNA samples using PCR
914 amplification. For every PCR reactions, we included a negative
915 control (distilled H₂O) and a positive control (1 L of purified OtV6).
916 PCR reactions were performed in 25 µL total volume using GoTaq®
917 Green Master Mix with 1 µL of RNA sample. Cycling reactions were
918 as follows: 5 m at 95 °C, followed by 35 cycles of 30 s at 95 °C, 30 s
919 at 50 °C, 45 s at 72 °C and with an additional 10 m extension at 72
920 °C. The PCR reactions were checked on 1% agarose gel stained with
921 GelRed™. The RT-PCR reactions were conducted using OneTaq®
922 One-Step RT-PCR (Qiagen). 1 µL of RNA was mixed in 50 µL
923 with 10 µL of Buffer 5×, 2 µL of 10 mM dNTP, 1 µL of each primer
924 (0.2 mM final concentration), 2 µL enzyme mix and finally 0.25 µL
925 of RNaseOUT™ (10 u/µL; Invitrogen, Life Technologies, Carlsbad,
926 CA, USA). Negative controls were made with 1 µL of water instead
927 of the RNA samples. Each PCR amplification was checked on 1%
928 agarose gel stained with GelRed™. Positive RT-PCRs were cloned
929 using Strataclone™ PCR cloning kit; one clone per library was
930 selected and double strand sequenced using *M13* primers.

931 **Cloning and functional analysis of vAmt in yeast.** The vAmt ORF
932 was synthesized *de novo* by Genscript (Piscataway, NJ, USA), codon
933 optimized for expression in *S. cerevisiae*, and fused to a C-terminal
934 GFP tag in vector p426 GPD. For complementation assays, the
935 vAmt ORF was amplified with primers *vAmt-attF/R* (Table S1)
936 using Phusion® polymerase (New England Biolabs, Ipswich, MA,
937 USA) to remove the GFP coding region; cloned into pDONR221
938 using Gateway® recombination (Life Technologies) and mobilized
939 into pAG416 GPD (low copy constitutive expression vector). For

931 fluorescence microscopy, the ORF was mobilized into pAG426 GPD
932 EGFP (N-terminal EGFP vector) or the original p426 GPD EGFP
933 (C-terminal) construct was used.

934 For yeast transformations, competent cells were prepared as
935 described in Thomson et al. [99], mixed with ~500 ng of plasmid
936 DNA, and pulsed at 1.5 kV in an Eppendorf electroporator. *S.*
937 *cerevisiae* strain 31019b was transformed with pAG416 GPD vAmt
938 or pAG416 GPD empty vector, as described above. Transformed
939 yeast 31019b cultures were grown to stationary phase at 30 °C
940 and centrifuged at 3200 × *g* for 2 m, washed twice in water and
941 diluted to OD_{600nm} 0.1 in 10 mL YNB liquid medium (0.19%
942 Yeast Nitrogen Base without amino acids and without (NH₄)₂SO₄;
943 Formedium, Norfolk, UK) containing a final concentration of 0.1
944 or 0.5 mM (NH₄)₂SO₄, D-mannosamine, D-glucuronamide or D,L-
945 a-amino-butyric Acid. Cells were then incubated at 30 °C and
946 OD_{600nm} measurements were taken at 24 h intervals. This method
947 was also used to assess growth of *S. cerevisiae* YNVW1 (Δ *dur3*)
948 and Σ 23346c (wild type) on urea, with YNB supplemented with
949 urea (0.1 – 2 mM) instead of (NH₄)₂SO₄. R v3 and *ggplot2* [100]
950 were used for statistical analyses and plots.

951 **Spinning disc confocal microscopy.** GFP constructs were trans-
952 formed into *S. cerevisiae* strain BY4742, as described above, grown
953 to mid-log phase and suspended in PBS. Spinning disc confocal
954 microscopy of EGFP-labelled cells was performed using an Olym-
955 pus IX81 inverted microscope and CSU-X1 Spinning Disc unit
956 (Yokogawa, Tokyo, Japan). A ×60/1.35 oil or ×100/1.40 oil objec-
957 tive was used with a 488 nm solid-state laser to excite the EGFP
958 fluorophore. A Photometrics® CoolSNAP™ HQ2 camera (Roper
959 Scientific, Martinsried, Germany) was used for imaging with the
960 VisiView® software (Visitron Systems, Puchheim, Germany).

961 **Transporter protein phenotyping.** To prepare cells for OmniLog®
962 Phenotype Microarray (PM) plates (Biolog, Hayward, CA, USA), each
963 yeast strain (*S. cerevisiae* 31019b transformed with either pAG416
964 GPD or pAG416 GPD vAmt) was grown on YNB+KNO₃-ura at
965 30 °C for 48 - 72 h. Colonies were suspended in Yeast Nutrient
966 Supplement solution (Biolog) and adjusted to 62% turbidity. 250
967 µL of cell suspension was made up to a final volume of 12 mL
968 of inoculating fluid, containing 1× IFY-0, 1× Dye Mix D, 50 mM
969 D-glucose, 1 mM disodium pyrophosphate and 2 mM sodium sulfate
970 and 100 µL was inoculated into each well of a PM3 MicroPlate™
971 (N sources). Assays were run in triplicate using independently ob-
972 tained transformants. OmniLog® Phenotype Microarray outputs
973 were analyzed by normalizing each individual plate against well A01
974 (negative control) to control for any background growth as a result
975 of the inoculation solution, then analyzed using the R package *opm*
976 [101]. Data were aggregated using the 'opm-fast' method, analyzed
977 using the area under curve (AUC) parameter and tested by t-test to
978 detect significant increase in respiration rates in the pAG416 GPD
979 vAmt strain.

980 **Yeast methylammonium uptake assays.** *S. cerevisiae* strains were
981 grown in 25 mL minimal proline medium [102] for 16 h at 30 °C
982 shaking. Cells were then diluted and grown until early log-phase
983 and harvested by centrifugation at 1000 × *g* for 3 m. Cells were
984 washed once and suspended in 2 mL medium lacking proline. The
985 dry weight of each sample was noted, before 90 µL aliquots of cells
986 were exposed to 5 concentrations (5 – 500 µM) of methylamine [¹⁴C]
987 hydrochloride for 1 m at 24 °C. Reactions were stopped by the
988 addition of 1 mL 120 mM methylamine hydrochloride. Background
989 adsorption was also calculated by exposing cells to 1 mL of 120
990 mM unlabeled methylamine hydrochloride prior to the addition of
991 the radiolabeled substrate. Cells were collected by centrifugation at
992 14000 × *g* for 3 m, washed and suspended in 500 µL deionized water,
993 then radioactivity was determined by liquid scintillation counting in
994 a liquid scintillation analyzer (LS 6500; Beckman Coulter, Brea, CA,
995 USA) after addition of 2.5 mL Emulsifier-Safe™ scintillation cocktail
996 solution (Perkin Elmer, Waltham, MA, USA). The R package *drc*
997 [103] was used to calculate Michaelis-Menten kinetics and curves.

998 **Infection timecourse experiments.** Two 15 mL cultures of *O. tauri*
999 were inoculated with OtV6 viruses and the infection was allowed
1000 to proceed until culture bleaching after 5 days. Cell debris were
removed by centrifugation at 3200 × *g* for 20 m followed by filtering

993 through a 0.2 µm syringe filter. Viruses were concentrated 10-fold
 994 using a 50 kDa Amicon® Ultra-15 Centrifugal Filter (Merck Milli-
 995 pore, Darmstadt, Germany) followed by a centrifugation at 3200 ×
 996 *g* for 2.5 m. 18 mL *O. tauri* cultures were cultured using 10 mL pre-
 997 culture and 8 mL media, 2 days prior to the experiment. To begin
 998 the infection timecourse experiments, 750 µL OtV6 were added and
 999 at each timepoint, 1 mL sample was pelleted and frozen in liquid
 1000 nitrogen for RNA preservation and the supernatant was stored at
 1001 -80 °C for fluorometric NH₄⁺ detection. Two 200 µL samples were
 1002 also taken for flow cytometry: i) 2 µL 25% glutaraldehyde were
 1003 added and the sample incubated for 15 m before freezing in liquid
 1004 nitrogen for *O. tauri* counts; ii) 8 µL 25% glutaraldehyde were
 1005 added and the sample incubated for 30 m at 4 °C before freezing
 1006 for viral counts. *O. tauri* and VLP abundances were monitored
 1007 by a FACSCanto™ flow cytometer (BD Biosciences, San Jose, CA,
 1008 USA) according to their right-angle scatter and the fluorescence
 1009 emission due either to the chlorophyll *a* pigment for *O. tauri* [104]
 1010 or to SYBR® Green I (Roche Diagnostics, Penzberg, Germany)
 1011 staining for VLPs [105]. A 900 µL sample was also removed for
 1012 assessing methylammonium uptake at each timepoint. Cells were
 1013 harvested by centrifugation at 5000 × *g* for 3 m and suspended in
 1014 450 µL media. For each sample, uptake rate for methylamine [¹⁴C]
 1015 hydrochloride was determined as aforementioned. The orthophthal-
 1016 dialdehyde (OPA) method [106] was used for fluorometric NH₄⁺
 1017 detection in cell-free medium (supernatant, see above). 20 µL of the
 1018 working reagent (OPA, borate buffer and sodium sulfite) was added
 1019 to 80 µL of the culture sample (or NH₄⁺ standard); samples and
 1020 standards were processed on a 96-well plate, which was incubated
 1021 in the dark at 25 °C with shaking for 2 - 3 h. Fluorescence was
 1022 then read at 355 nm excitation and 420 nm emission on an Infinite®
 1023 M200 plate reader (Tecan, Männedorf, Switzerland).

1024 **Quantitative PCR.** RNA was extracted using the RNeasy® Plus Uni-
 1025 versal Mini kit (Qiagen) following the manufacturer's instructions
 1026 and incorporating a 5 m elution step using 30 µL RNase-free water.
 1027 Residual DNA was removed using the Turbo DNA-free™ kit (Am-
 1028 bion, Life Technologies) and 6 µL RNA reverse-transcribed using
 1029 the Superscript® III First Strand Synthesis SuperMix (Invitrogen)
 1030 and oligo(dT)₂₀ primers, following the manufacturer's instructions.
 1031 cDNA was quantified using a Qubit™ ssDNA Assay Kit (Life Tech-
 1032 nologies) and stored at -20 °C prior to performing qPCR. Plasmids
 1033 for each gene of interest were generated by Phusion® polymerase
 1034 (New England Biolabs) PCR using cDNA templates, followed by
 1035 A-tailing using Taq polymerase and cloning using a Strataclone™
 1036 PCR cloning kit (Agilent Technologies). Each plasmid was con-
 1037 firmed by sequencing (Eurofins Genomics) and serial dilutions (10⁸
 1038 - 10 copies) were used to generate standard curves for each primer
 1039 pair and probe. Efficiencies ranged from 96 - 102% (Table S4).
 1040 qPCR reactions were performed in a StepOnePlus™ Real-Time
 1041 PCR system (Thermo Fisher Scientific, Waltham, MA, USA). Each
 1042 25 µL reaction contained 12.5 µL TaqMan™ Gene Expression Mas-
 1043 ter Mix (Thermo Fisher Scientific), 900 nM each primer, 250 nM
 1044 hydrolysis probe and 1 µL cDNA/plasmid DNA and was performed
 1045 in duplicate alongside no-template and minus-RT controls. Cycling
 1046 conditions were as follows: UDG activation for 2 m at 50 °C and
 1047 DNA polymerase activation for 10 m at 95 °C, followed by 40 cycles
 1048 of 15 s at 95 °C and 1 m at 60 °C. ROX was used as an internal
 1049 reference dye for analysis of CT values, which were determined using
 1050 StepOne™ Software v2.3 (Thermo Fisher Scientific), and standard
 1051 curves were used for quantification of each gene.

1052 **Data access.** Phylogenetic and experimental data are available at
 1053 Zenodo: zenodo.org/record/61901. PCR-amplified sequence assem-
 1054 bly of the vAmt locus was deposited in GenBank (KX254356).

1055 **ACKNOWLEDGMENTS.** AM and TAR are funded by the Royal
 1056 Society, through Newton and University Research fellowships, re-
 1057 spectively. This work is supported in part by research grants from
 1058 Natural Environmental Research Council, The Gordon and Betty
 1059 Moore Foundation, Leverhulme Trust and the University of Exeter.
 1060 The University of Exeter OmniLog® facility is supported by a Well-
 1061 come Trust Institutional Strategic Support Award WT105618MA.
 1062 Phylogenetic reconstructions were computed on the Data Inten-
 1063 sive Academic Grid (National Science Foundation, MRI-R2 project

#DBI-0959894). We thank C. Salmeron and the cytometry platform
 BioPIC (OOB, Banyuls), as well as C. Lambert and the LEMAR cy-
 tometry core facilities (IUEM, Brest) for assistance in FCM counts.
 We are grateful to Dr. A.-M. Marini (Université Libre de Bruxelles)
 and to Dr. G. P. Bienert (Leibniz Institute of Plant Genetics and
 Crop Plant Research) for yeast mutant strains. We thank Prof. K.
 Haynes, Dr. F. Maguire, Dr. F. Savory, Prof. N. Smirnov and Dr.
 J. G. Wideman (University of Exeter) for helpful comments.

1. Falkowski P (2012) Ocean science: the power of plankton. *Nature* 483(7387):S17–S20. 1062
2. Arrigo KR (2005) Marine microorganisms and global nutrient cycles. *Nature* 437(7057):349–355. 1063
3. Moore C et al. (2013) Processes and patterns of oceanic nutrient limitation. *Nat Geosci* 6(9):701–710. 1064
4. Litchman E, Klausmeier CA, Schofield OM, Falkowski PG (2007) The role of functional traits and trade-offs in structuring phytoplankton communities: scaling from cellular to ecosystem level. *Ecol Lett* 10(12):1170–1181. 1065
5. Hildebrand M (2005) Cloning and functional characterization of ammonium transporters from the marine diatom *Cylindrotheca fusiformis* (Bacillariophyceae). *J Phycol* 41(1):105–113. 1066
6. Allen AE, Vardi A, Bowler C (2006) An ecological and evolutionary context for integrated nitrogen metabolism and related signaling pathways in marine diatoms. *Curr Opin in Plant Biol* 9(3):264–273. 1067
7. McDonald SM, Plant JN, Worden AZ (2010) The mixed lineage nature of nitrogen transport and assimilation in marine eukaryotic phytoplankton: a case study of *Micromonas*. *Mol Biol Evol* 27(10):2268–2283. 1068
8. Dagenais-Bellefeuille S, Morse D (2013) Putting the N in dinoflagellates. *Front Microbiol* 4:369. 1069
9. Terrado R, Monier A, Edgar R, Lovejoy C (2015) Diversity of nitrogen assimilation pathways among microbial photosynthetic eukaryotes. *J Phycol* 51(3):490–506. 1070
10. Mulholland MR, Lomas MW (2008) Nitrogen uptake and assimilation in *Nitrogen in the marine environment*, eds. Capone D, Bronk D, Mulholland M, Carpenter E. (Academic Press, New York, NY), pp. 303–384. 1071
11. Gilbert PM et al. (2016) Pluses and minuses of ammonium and nitrate uptake and assimilation by phytoplankton and implications for productivity and community composition, with emphasis on nitrogen-enriched conditions. *Limnol Oceanogr* 61(1):165–197. 1072
12. Gobler CJ et al. (2011) Niche of harmful alga *Aureococcus anophagefferens* revealed through ecogenomics. *Proc Natl Acad Sci USA* 108(11):4352–4357. 1073
13. Worm B, Lotze HK, Hillebrand H, Sommer U (2002) Consumer versus resource control of species diversity and ecosystem functioning. *Nature* 417(6891):848–851. 1074
14. Pasulka AL, Samo TJ, Landry MR (2015) Grazer and viral impacts on microbial growth and mortality in the Southern California Current Ecosystem. *J Plankton Res* p. fbv011. 1075
15. Suttle CA (2007) Marine viruses—major players in the global ecosystem. *Nature Rev Microbiol* 5(10):801–812. 1076
16. Brussaard CP (2004) Viral control of phytoplankton populations — a review. *J Eukaryot Microbiol* 51(2):125–138. 1077
17. Rohwer FV, Thurber RV (2009) Viruses manipulate the marine environment. *Nature* 459(7244):207–212. 1078
18. Wilhelm SW, Suttle CA (1999) Viruses and nutrient cycles in the sea. *Bioscience* 49(10):781–788. 1079
19. Breitbart M (2012) Marine viruses: truth or dare. *Annu Rev Mar Sci* 4:425–448. 1080
20. Hurwitz BL, Hallam SJ, Sullivan MB (2013) Metabolic reprogramming by viruses in the sunlit and dark ocean. *Genome Biol* 14(11):1. 1081
21. Roux S et al. (2016) Ecogenomics and potential biogeochemical impacts of globally abundant ocean viruses. *Nature* 537(7622):689. 1082
22. Monier A et al. (2009) Horizontal gene transfer of an entire metabolic pathway between a eukaryotic alga and its DNA virus. *Genome Res* 19(8):1441–1449. 1083
23. Thompson LR et al. (2011) Phage auxiliary metabolic genes and the redirection of cyanobacterial host carbon metabolism. *Proc Natl Acad Sci USA* 108(39):E757–E764. 1084
24. Dammeyer T, Bagby SC, Sullivan MB, Chisholm SW, Frankenberg-Dinkel N (2008) Efficient phage-mediated pigment biosynthesis in oceanic cyanobacteria. *Curr Biol* 18(6):442–448. 1085
25. Rosenwasser S et al. (2014) Rewiring host lipid metabolism by large viruses determines the fate of *Emiliania huxleyi*, a bloom-forming alga in the ocean. *Plant Cell* 26(6):2689–2707. 1086
26. Malitsky S et al. (2016) Viral infection of the marine alga *Emiliania huxleyi* triggers lipidome remodeling and induces the production of highly saturated triacylglycerol. *New Phytol* 210(1):88–96. 1087
27. Ziv C et al. (2016) Viral serine palmitoyltransferase induces metabolic switch in sphingolipid biosynthesis and is required for infection of a marine alga. *Proc Natl Acad Sci USA* 113(13):E1907–E1916. 1088
28. Wilson WH, Carr NG, Mann NH (1996) The effect of phosphate status on the kinetics of cyanophage infection in the oceanic cyanobacterium *Synechococcus* sp. wh78031. *J Phycol* 32(4):506–516. 1089
29. Monier A et al. (2012) Phosphate transporters in marine phytoplankton and their viruses: cross-domain commonalities in viral-host gene exchanges. *Environ Microbiol* 14(1):162–176. 1090
30. Maat DS, Crawford KJ, Timmermans KR, Brussaard CP (2014) Elevated CO₂ and phosphate limitation favor *Micromonas pusilla* through stimulated growth and reduced viral impact. *Appl Environ Microbiol* 80(10):3119–3127. 1091
31. Maat DS, Brussaard CP (2016) Both phosphorus and nitrogen limitation constrain viral proliferation in marine phytoplankton. *Aquat Microb Ecol* 77(2):87–97. 1092
32. McDonald TR, Dietrich FS, Lutzoni F (2012) Multiple horizontal gene transfers of ammonium transporters/ammonia permeases from prokaryotes to eukaryotes: toward a new functional and evolutionary classification. *Mol Biol Evol* 29(1):51–60. 1093

1117 33. Mojica KD, Brussaard CP (2014) Factors affecting virus dynamics and microbial host–virus
1118 interactions in marine environments. *FEMS Microbiol Ecol* 89(3):495–515. 1180
1119 34. UniProt Consortium (2014) Activities at the universal protein resource (UniProt). *Nucleic
1120 Acids Res* 42(D1):D191–D198. 1181
1121 35. Andrade SL, Einsle O (2007) The Amt/Mep/Rh family of ammonium transport proteins. *Molec
1122 Membrane Biol* 24(5-6):357–365. 1182
1123 36. von Wirén N, Gazzarrini S, Gojon A, Frommer WB (2000) The molecular physiology of
1124 ammonium uptake and retrieval. *Curr Opin Plant Biol* 3(3):254–261. 1183
1125 37. Iyer LM, Aravind L, Koonin EV (2001) Common origin of four diverse families of large eu-
1126 karyotic DNA viruses. *J Virol* 75(23):11720–11734. 1184
1127 38. Short SM (2012) The ecology of viruses that infect eukaryotic algae. *Environ Microbiol*
1128 14(9):2253–2271. 1185
1129 39. Marin B, Melkonian M (2010) Molecular phylogeny and classification of the Mamiello-
1130 phyceae class. nov.(Chlorophyta) based on sequence comparisons of the nuclear-and
1131 plastid-encoded rRNA operons. *Protist* 161(2):304–336. 1186
1132 40. Monier A, Worden AZ, Richards TA (2016) Phylogenetic diversity and biogeography of the
1133 Mamiellophyceae lineage of eukaryotic phytoplankton across the oceans. *Environ Microbiol
1134 Rep* 8(4):461–469. 1187
1135 41. Derelle E et al. (2008) Life-cycle and genome of OtV5, a large DNA virus of the pelagic
1136 marine unicellular green alga *Ostreococcus tauri*. *PLoS One* 3(5):e2250. 1188
1137 42. Weynberg KD, Allen MJ, Ashelford K, Scanlan DJ, Wilson WH (2009) From small hosts come
1138 big viruses: the complete genome of a second *Ostreococcus tauri* virus, OtV-1. *Environ
1139 Microbiol* 11(11):2821–2839. 1189
1140 43. Weynberg KD, Allen MJ, Gilg IC, Scanlan DJ, Wilson WH (2011) Genome sequence of
1141 *Ostreococcus tauri* virus OtV-2 throws light on the role of picoeukaryote niche separation in
1142 the ocean. *J Virol* 85(9):4520–4529. 1190
1143 44. Thomas R et al. (2011) Acquisition and maintenance of resistance to viruses in eukaryotic
1144 phytoplankton populations. *Environ Microbiol* 13(6):1412–1420. 1191
1145 45. Moreau H et al. (2010) Marine prasinovirus genomes show low evolutionary divergence and
1146 acquisition of protein metabolism genes by horizontal gene transfer. *J Virol* 84(24):12555–
1147 12563. 1192
1148 46. Derelle E et al. (2015) Diversity of viruses infecting the green microalga *Ostreococcus luci-
1149 marinus*. *J Virol* 89(11):5812–5821. 1193
1150 47. Derelle E et al. (2006) Genome analysis of the smallest free-living eukaryote *Ostreococcus
1151 tauri* unveils many unique features. *Proc Natl Acad Sci USA* 103(31):11647–11652. 1194
1152 48. Monier A et al. (2008) Marine mimivirus relatives are probably large algal viruses. *Virol J*
1153 5(1):12. 1195
1154 49. Monier A, Claverie JM, Ogata H (2008) Taxonomic distribution of large DNA viruses in the
1155 sea. *Genome Biol* 9(7):1. 1196
1156 50. Hingamp P et al. (2013) Exploring nucleocytoplasmic large DNA viruses in *Tara Oceans*
1157 microbial metagenomes. *ISME J* 7(9):1678–1695. 1197
1158 51. Loqué D et al. (2006) Additive contribution of AMT1; 1 and AMT1; 3 to high-affinity am-
1159 monium uptake across the plasma membrane of nitrogen-deficient *Arabidopsis* roots. *Plant J*
1160 48(4):522–534. 1198
1161 52. Khademi S et al. (2004) Mechanism of ammonia transport by Amt/MEP/Rh: structure of
1162 AmtB at 1.35 Å. *Science* 305(5690):1587–1594. 1199
1163 53. Zheng L, Kostrewa D, Bernéche S, Winkler FK, Li XD (2004) The mechanism of ammonia
1164 transport based on the crystal structure of AmtB of *Escherichia coli*. *Proc Natl Acad Sci
1165 USA* 101(49):17090–17095. 1200
1166 54. Andrade SL, Dickmanns A, Figner R, Einsle O (2005) Crystal structure of the archaeal
1167 ammonium transporter Amt-1 from *Archaeoglobus fulgidus*. *Proc Natl Acad Sci USA*
1168 102(42):14994–14999. 1201
1169 55. Javelle A et al. (2006) An unusual twin-his arrangement in the pore of ammonia channels is
1170 essential for substrate conductance. *J Biol Chem* 281(51):39492–39498. 1202
1171 56. Marini AM, Soussi-Boudekou S, Vissers S, André B (1997) A family of ammonium trans-
1172 porters in *Saccharomyces cerevisiae*. *Mol Cell Biol* 17(8):4282–4293. 1203
1173 57. Liu LH, Ludewig U, Frommer WB, von Wirén N (2003) AtDUR3 encodes a new type of
1174 high-affinity urea/H⁺ symporter in *Arabidopsis*. *Plant Cell* 15(3):790–800. 1204
1175 58. Bu Y et al. (2013) Identification and characterization of a PutAMT1; 1 gene from *Puccinellia
1176 tenuiflora*. *PLoS One* 8(12):e83111. 1205
1177 59. Bochner BR (2009) Global phenotypic characterization of bacteria. *FEMS Microbiol Rev*
1178 33(1):191–205. 1206
1179 60. Brown CM, Bidle KD (2014) Attenuation of virus production at high multiplicities of infection
1180 in *Aureococcus anophagefferens*. *Virology* 466:71–81. 1207
1181 61. Keeling PJ et al. (2014) The Marine Microbial Eukaryote Transcriptome Sequencing Project
1182 (MMETSP): illuminating the functional diversity of eukaryotic life in the oceans through tran-
1183 scriptome sequencing. *PLoS Biol* 12(6):e1001889. 1208
1184 62. Dinsdale EA et al. (2008) Functional metagenomic profiling of nine biomes. *Nature*
1185 452(7187):629–632. 1209
1186 63. Kettler GC et al. (2007) Patterns and implications of gene gain and loss in the evolution of
1187 *Prochlorococcus*. *PLoS Genet* 3(12):e231. 1210
1188 64. Richards TA, Talbot NJ (2013) Horizontal gene transfer in osmotrophs: playing with public
1189 goods. *Nature Rev Microbiol* 11(10):720–727. 1211
1190 65. Martiny AC, Treseder K, Pusch G (2013) Phylogenetic conservatism of functional traits in
1191 microorganisms. *ISME J* 7(4):830–838. 1212
1192 66. Ignacio-Espinoza JC, Sullivan MB (2012) Phylogenomics of 14 cyanophages: lateral gene
1193 transfer in the ‘core’ and origins of host genes. *Environ Microbiol* 14(8):2113–2126. 1213
1194 67. Millard A, Clokie MR, Shub DA, Mann NH (2004) Genetic organization of the *psbAD* region
1195 in phages infecting marine *Synechococcus* strains. *Proc Natl Acad Sci USA* 101(30):11007–
1196 11012. 1214
1197 68. Lindell D et al. (2004) Transfer of photosynthesis genes to and from *Prochlorococcus* viruses.
1198 *Proc Natl Acad Sci USA* 101(30):11013–11018. 1215
1199 69. Sullivan MB et al. (2006) Prevalence and evolution of core photosystem II genes in marine
1200 cyanobacterial viruses and their hosts. *PLoS Biol* 4(8):e234. 1216
1201 70. Worden AZ, Nolan JK, Palenik B, et al. (2004) Assessing the dynamics and ecology of
1202 marine picophytoplankton: the importance of the eukaryotic component. *Limnol Oceanogr*
1203 49(1):168–179. 1217
1204 71. Stevenson R, Silver S (1977) Methylammonium uptake by *Escherichia coli*: evidence for a
1205 bacterial NH₄⁺ transport system. *Biochem Biophys Res Commun* 75(4):1133–1139. 1218
1206 72. Johnson DA et al. (2008) High-throughput phenotypic characterization of *Pseudomonas
1207 aeruginosa* membrane transport genes. *PLoS Genet* 4(10):e1000211. 1219
1208 73. Cheng YS, Labavitch J, VanderGheynst JS (2015) Organic and inorganic nitrogen impact
1209 *Chlorella variabilis* productivity and host quality for viral production and cell lysis. *Appl
1210 Biochem Biotechnol* 176(2):467–479. 1220
1211 74. Jover LF, Effler TC, Buchan A, Wilhelm SW, Weitz JS (2014) The elemental composition
1212 of virus particles: implications for marine biogeochemical cycles. *Nature Rev Microbiol*
1213 12(7):519–528. 1221
1214 75. Clasen JL, Elser JJ (2007) The effect of host *Chlorella* NC64A carbon: phosphorus ratio on
1215 the production of *Paramecium bursaria Chlorella* virus-1. *Freshwater Biol* 52(1):112–122. 1222
1216 76. Nissimov JI, Napier JA, Allen MJ, Kimmance SA (2016) Intragener competition between
1217 coccolithoviruses: an insight on how a select few can come to dominate many. *Environ
1218 Microbiol* 18(1):133–145. 1223
1219 77. Maat DS, van Bleijswijk JD, Witte HJ, Brussaard CP (2016) Virus production in phosphorus-
1220 limited *Micromonas pusilla* stimulated by a supply of naturally low concentrations of different
1221 phosphorus sources, far into the lytic cycle. *FEMS Microbiol Ecol* 92(9):fiw136. 1224
1222 78. Wilson W, Van Etten JL, Allen M (2009) The Phycodnaviridae: the story of how tiny giants
1223 rule the world in *Lesser Known Large dsDNA Viruses*, ed. Van Etten JL. (Springer-Verlag,
1224 Berlin-Heidelberg, Germany), pp. 1–42. 1225
1225 79. Colson P et al. (2011) Viruses with more than 1,000 genes: Mamavirus, a new *Acan-
1226 thamoeba polyphaga* mimivirus strain, and reannotation of Mimivirus genes. *Genome Biol
1227 Evol* 3:737–742. 1226
1228 80. Sullivan MB et al. (2010) Genomic analysis of oceanic cyanobacterial myoviruses com-
1229 pared with T4-like myoviruses from diverse hosts and environments. *Environ Microbiol*
1230 12(11):3035–3056. 1227
1231 81. Sharon I et al. (2009) Photosystem I gene cassettes are present in marine virus genomes.
1232 *Nature* 461(7261):258–262. 1228
1233 82. Anantharaman K et al. (2014) Sulfur oxidation genes in diverse deep-sea viruses. *Science*
1234 344(6185):757–760. 1229
1235 83. Zeng Q, Chisholm SW (2012) Marine viruses exploit their host’s two-component regulatory
1236 system in response to resource limitation. *Curr Biol* 22(2):124–128. 1230
1237 84. NCBI Resource Coordinators (2015) Database resources of the National Center for Biotech-
1238 nology Information. *Nucleic Acids Res* 43(D1):D6. 1231
1239 85. Eddy SR (2011) Accelerated profile HMM searches. *PLoS Comput Biol* 7(10):e1002195. 1232
1240 86. Finn RD et al. (2013) Pfam: the protein families database. *Nucleic Acids Res* p. gkt1223. 1233
1241 87. Haft DH, Selengut JD, White O (2003) The TIGRFAMs database of protein families. *Nucleic
1242 Acids Res* 31(3):371–373. 1234
1243 88. Krogh A, Larsson B, Von Heijne G, Sonnhammer EL (2001) Predicting transmembrane pro-
1244 tein topology with a hidden Markov model: application to complete genomes. *Journal Mol
1245 Biol* 305(3):567–580. 1235
1246 89. Zhang Y (2008) I-TASSER server for protein 3D structure prediction. *BMC Bioinformatics*
1247 9(1):1. 1236
1248 90. Meng EC, Pettersen EF, Couch GS, Huang CC, Ferrin TE (2006) Tools for integrated
1249 sequence-structure analysis with UCSF Chimera. *BMC Bioinformatics* 7(1):1. 1237
1250 91. Price MN, Dehal PS, Arkin AP (2010) FastTree 2 –approximately maximum-likelihood trees
1251 for large alignments. *PLoS One* 5(3):e9490. 1238
1252 92. Camacho C et al. (2009) BLAST+: architecture and applications. *BMC Bioinformatics*
1253 10(1):1. 1239
1254 93. Katoh K, Standley DM (2013) MAFFT multiple sequence alignment software version 7: im-
1255 provements in performance and usability. *Mol Biol Evol* 30(4):772–780. 1240
1256 94. Capella-Gutiérrez S, Silla-Martínez JM, Gabaldón T (2009) trimAl: a tool for automated
1257 alignment trimming in large-scale phylogenetic analyses. *Bioinformatics* 25(15):1972–1973. 1241
1258 95. Stamatakis A (2014) RAxML version 8: a tool for phylogenetic analysis and post-analysis of
1259 large phylogenies. *Bioinformatics* 30(9):1312–1313. 1242
1260 96. Darriba D, Taboada GL, Doallo R, Posada D (2011) ProtTest 3: fast selection of best-fit
1261 models of protein evolution. *Bioinformatics* 27(8):1164–1165. 1243
1262 97. Hurwitz B (2014) iMicrobe: Advancing clinical and environmental microbial research using
1263 the iPlant cyberinfrastructure in *Plant and Animal Genome XXII Conference*. (Plant and
1264 Animal Genome, San Diego, CA, USA). 1244
1265 98. Matsen FA, Kodner RB, Armbrust EV (2010) pplacer: linear time maximum-likelihood and
1266 bayesian phylogenetic placement of sequences onto a fixed reference tree. *BMC Bioinform-
1267 atics* 11(1):1. 1245
1268 99. Thompson JR, Register E, Curotto J, Kurtz M, Kelly R (1998) An improved protocol for the
1269 preparation of yeast cells for transformation by electroporation. *Yeast* 14(6):565–571. 1246
1270 100. Wickham H (2009) *ggplot2: elegant graphics for data analysis*. (Springer Science & Busi-
1271 ness Media). 1247
1272 101. Vaas LA et al. (2013) opm: an R package for analysing OmniLog® phenotype microarray
1273 data. *Bioinformatics* 29(14):1823–1824. 1248
1274 102. Jacobs P, Jauniaux JC, Grenson M (1980) A cis-dominant regulatory mutation linked to the
1275 argb-argc gene cluster in *Saccharomyces cerevisiae*. *J Mol Biol* 139(4):691–704. 1249
1276 103. Ritz C, Streibig JC, et al. (2005) Bioassay analysis using r. *J Stat Softw* 12(5):1–22. 1250
1277 104. Trask B, Van den Engh G, Elgershuizen J (1982) Analysis of phytoplankton by flow cytometry.
1278 *Cytometry* 2(4):258–264. 1251
1279 105. Brussaard CP (2004) Optimization of procedures for counting viruses by flow cytometry.
1280 *Appl Environ Microb* 70(3):1506–1513. 1252
1281 106. Holmes RM, Aminot A, Kérouel R, Hooker BA, Peterson BJ (1999) A simple and precise
1282 method for measuring ammonium in marine and freshwater ecosystems. *Can J Fish Aquat
1283 Sci* 56(10):1801–1808. 1253
1284 1254

